Design and Implementation of a Chaotic Unipolar Sine-Pulse Modulation Technique for a transformerless single-phase Grid-Connected Photovolatic Inverter

Sana Kraiem (kraiem.sana5@gmail.com)
ENISo: Ecole Nationale d'Ingenieurs de Sousse https://orcid.org/0000-0001-9770-5397

Research Article

Keywords: Chaotic, SPWM, PV inverters, grid-connected, Total Harmonic Distortion (THD), Electromagnetic Interference (EMI)

Posted Date: May 9th, 2022

DOI: https://doi.org/10.21203/rs.3.rs-1626697/v1

Design and Implementation of a Chaotic Unipolar Sine-Pulse Modulation Technique for a transformerless single-phase Grid-Connected Photovolatic Inverter

S. Kraiem[1], M. Hamouda[2], J. Ben Hadj Slama[3]

University of Sousse, National engineering school of Sousse, LATIS- Laboratory of Advanced Technology and Intelligent Systems, 4023, Sousse, Tunisia;
[1]Kraiem.sana5@gmail.com, [2]mahmoudhamouda@yahoo.fr, [3]bhslama@yahoo.fr

Abstract-*Transformerless grid-connected inverters for photovoltaic (PV) applications provide several advantages such as reduced cost and volume as well as an increased efficiency. However, the removal of the transformer gives rise to several problems related to leakage currents and electromagnetic interferences (EMI). This paper presents different chaotic unipolar sine-pulse width modulation (C-USPWM) techniques for a transformerless grid-connected PV inverter based on parameter selection. The main objective behind this proposed chaotic modulation technique is to reduce the conducted EMI without worsening the power quality and the common mode voltage (CMV). The method is validated through numerical simulations and experimental tests carried out on laboratory prototype of an optimized H5 inverter (oH5). The obtained results showed its superiority to the conventional unipolar sine-pulse width modulation (USPWM). We showed also that the appropriate parameter selection of the C-UPSWM could advantageously combine an improved EMI performance and an efficient control, making it possible to deliver a significant reduction of the peaks' amplitudes in the frequency spectrum of the common-mode (CM) voltage.*

Keywords Chaotic, SPWM, PV inverters, grid-connected, Total Harmonic Distortion (THD), Electromagnetic Interference (EMI).

1. Introduction

PV systems have successfully been connected to the grid for generating renewable energy for residential buildings. In these installations, to reduce system cost and enhance its efficiency, it is common to eliminate the transformer in PV inverter topologies [1], [2]. Nonetheless, the removal of the transformer can cause a fluctuation of the common-mode (CM) voltage that leads to a high leakage current through the stray capacitors. In recent years, CM current reduction topologies have been proposed in the literatures [3-6], such as H5 and optimized H5 (oH5). However, these topologies use an important number of power semiconductors that cause several problems such as circuit design complications, serious harmonic distortion, and electromagnetic interference (EMI) issues [7]. It has been proven that the EMI at low frequencies is mostly determined by the Pulse Width Modulation (PWM) strategies of power semiconductor devices [8]. Further, the switching transients of these devices considerably affect the EMI at high frequencies. To enable the final product to meet the requirements of electromagnetic compatibility (EMC) standards, the EMI suppression is adopted before or after the converter design process. After the converter construction phase, filters can be applicable to attenuate the conducted EMI along propagation paths. However, it is bulky and expensive due to the weight and size of the reactive elements of EMI filters. At the early stage, the EMI can be eliminated from the source of their creation [8]. This EMI reduction approach can be divided into three groups: component selection, soft switching, printed circuit board (PCB) design, layout [9], and switch control scheme [10].

Hence, for instance in renewable energy systems, designers pay a lot of attention to PCB layout optimization, components selection, EMI filters and shielding efficiency studies [11], [12]. However, far less work has been conducted to improve pulse width modulation (PWM) techniques, with the aim of reducing EMI of power electronic converters [13], [14]. These techniques are classified as bipolar and unipolar sine pulse width modulations (BSPWM and USPWM). Indeed, BSPWM produces large switching losses and reduce the inverter efficiency. However, the conventional USPWM offers less current ripple, which reduced switching losses and can generate less EMI. Most of research works have revealed that due to the constant switching frequency, significant peaks of EMI are concentrated on multiples of this switching frequency [15]. Nevertheless, in order to spread the harmonic peaks over a wide frequency band, a variable switching frequency is preferred [16] [17]. Within this context, a chaotic USPWM (C-USPWM) introduces a random behaviour using the chaos control concept. Since the external chaotic signal is conducted by a chaotic dynamics, the chaotic USPWM technique facilitates the design of power converters, provides more flexibility and a better spectral performance [18] [19].

This paper proposes a chaotic unipolar sine-pulse width modulation (C-USPWM) technique for a transformerless single-phase grid-connected PV inverter. The aim of this proposed C-USPWM technique is to reduce the conducted EMI and preserve good performance in terms of injected grid current quality (THD) and CMV. The proposal is validated with numerical simulations carried out on a circuit-type software as well as experimental tests on a scaled-down laboratory prototype of an oH5 PV inverter. The obtained results confirm that this method can effectively reduce the conducted EMI as compared to the conventional UPSPWM. The results showed also the capability of the chaotic technique in reducing the

voltage's THD and conducted EMI level, through an appropriate selection of the C-USPWM parameters.

The remaining of this paper is organized as follows: Section 2 is devoted to the presentation of the conventional USPWM. Then chaotic modulation technique is investigated. Section 4 provides a Chaotic USPWM real time implementation. Section 5 concludes this paper.

2. Conventional Unipolar SPWM

High common mode voltages and currents flowing through circuits in PV systems usually have electrical isolation issues, which is a very crucial topic. Indeed, the galvanic separation is the common technique to remove undesired effects of leakage currents and prevent dangerous harmonics to be transmitted in the grid. This is achieved using an isolation transformer and a clean wiring. However, recently, in PV grid connected systems, more attention is given to transformerless inverters since it has been demonstrated that the remove of the transformer offers much lighter weight and higher efficiencies. Yet, a direct connection between AC and DC sides creates a common-mode (CM) current circulation. It is also possible note that the variation of CM voltages electrify the resonant circuit and provoke even a higher leakage current through the ground, depending on the topology design and control strategies. Therefore, in order to minimize leakage current and keep a constant level of CMV, the design topology and the modulation scheme selection have to be given careful attention.

In the literature, several researches have addressed the CMV issues with the aim to reduce or eliminate the disturbing leakage current paths by proposing different modified FB topologies [1] [2]. In the present study, an oH5 inverter topology is suggested. It is the optimized topology of the most popular and widely known commercial transformerless single-phase PV structure [6]. In this topology, two additional power switches are implemented between the positive (or negative) DC pole and the PV array. This inverter is known as neutral-point-clamped topology.

Moreover, several PWM techniques have been proposed to optimize the inverter operations. Among these works, sinusoidal PWM (SPWM) is widely preferred because it allows a direct control of the inverter output voltage and the output frequency according to sine functions [20]. In general, sinusoidal sampling methods employed for PWM control are classified into two categories: unipolar (USPWM) and bipolar (BSPWM). Hence, we restrict the study for the scope of this paper to the use of the conventional USPWM technique.USPWM is a three-level modulation technique, generating three-level output voltages: + V_{PV}, 0, and – V_{PV}. In the inverter employing a conventional unipolar technique, two sinusoidal modulating waveforms, which are of the same magnitude and frequency but are in opposite phases, are required. These two are compared with a common high-frequency carrier waveform with a fixed switching frequency, as shown in Fig. 1. The switching frequency is defined by the fixed carrier frequency (f_r). During the switching activity, two pairs of switches S_3-S_4 (or S_1- S_2) are commuting at positive (or negative) half cycles with a fixed switching carrier period (T_c).

In the positive half cycle, when S3 and S4 are turned on: v_{AN} = V_{PV} /2 and v_{BN} = V_{PV} /2, then v_{CM}= V_{PV}/2, and when S3 and S4 are turned off: v_{CM} =V_{pv}/2. Similarly, for the negative half cycle. Hence, it is clear that USPWM with oH5 topology creates a constant CMV.

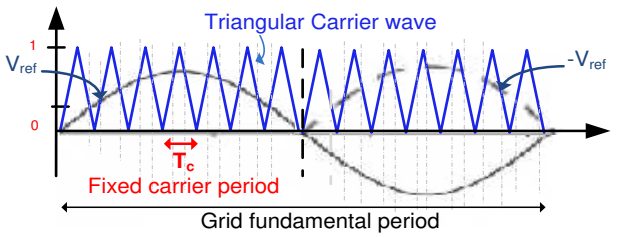

Fig. 1 Constant frequency of triangular carrier waveform for USPWM

In order to evaluate the impact of the proposed USPWM control strategies, a numerical simulation have been carried out based on a grid-tied oH5 inverter topology. The PV conversion system parameters are shown in Table I.

Table I. Configuration parameters of simulation tests

Parameters	Value
DC voltage, V_{dc}	400 V
Reference switching frequency, f_r	20 KHz
Grid voltage/frequency	220V/50Hz
Bus capacitor C_{dc}	470 µF
Parasitic capacitor: C_{PV1}, C_{PV2}	100 nF
Filter's capacitor, C_f	6.6 µF
Filter's inductors, L_f	5 mH

First, the electrical performance of the simulated model of the oH5 inverter topology is verified. Simulation results of the application of the conventional USPWM control strategy to the studied structure are given in Figs. 2. The obtained CM voltage in Fig.2 (b) is constant, and then CM current will be eliminated. Second, the spectra of the output voltage v_{AB} is provided using a fast Fourier transformation (FFT). Total harmonic distortion (THD) measuring the magnitude of the harmonic distortion is also provided for output voltage signals, as depicted in Fig. 2 (c). We observe the presence of several important harmonic pics over a frequency range that covers tens of kilohertz.

In this work, an EMI mitigation study performed on an oH5 transformerless PV inverter based on chaotic USPWM will be established.

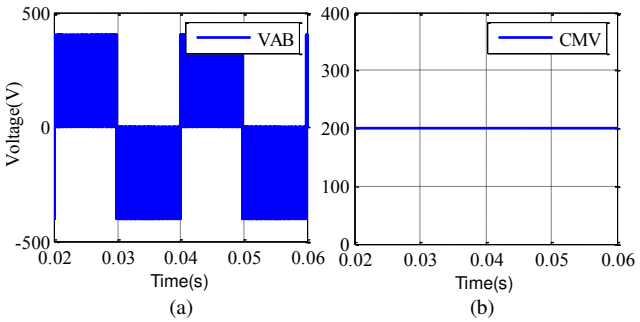

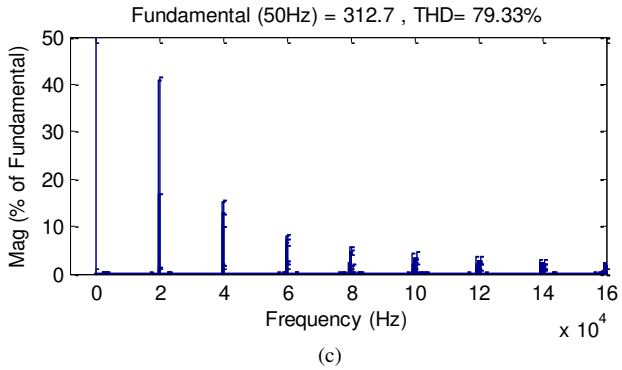

(c)

Fig.2 Obtained results under RUSPWM control: (a) modulated output voltage v_{AB}, (b) CMV, (c) frequency spectrum of v_{AB}

3. Chaotic modulation technique

In the literature, several researchers have studied the effect of chaotic PWM on reducing harmonics and improving the distribution of the frequency spectrum, particularly when dealing with power converters [18] [19]. It has been established that the chaotic modulated signal does not decrease performance, but even better, it offers lower EMI. Therefore, although the fact that chaotic behavior studies can be complex while the engineering design process, chaotic PWM is worthy for further researches and being used in practice. In the present work, a chaotic unipolar SPWM (C-USPWM) technique is proposed and implemented into the oH5 PV inverter, Fig. 3.

Regarding the pseudorandom characteristics of chaotic sequences, the varying carrier period T_i is changing chaotically under C-USPWM as follows:

$$T_i = T_r + \Delta T\, \varepsilon_i,\ \varepsilon_i \in [-1, 1],\ i = 1,2..N \qquad (1)$$

Where T_r is the reference period, ΔT is the maximum period offset, and ε_i is a chaotic series generated using the logistic mapping. It is noted that $Tc = \sum_{i=0}^{N} T_i$, and $\omega_c = 2\pi/Tc$ where $T_0 = 0$ and $Ti\ (i = 1, 2, 3\ldots N)$, with N is the number of carriers in one period, . In this work, parameters are defined as $T_r = \frac{1}{fr} = 50$ µs, $\Delta T = \beta Tr$ and for ε_i:

$$\gamma_i = r\,\gamma_{i-1}\,(1-\gamma_{i-1}),\ i = 1, 2\ldots, \gamma_i \in [0, 1],\ r \in [0,4] \qquad (2)$$

$$\varepsilon_i = 2(\gamma_i - 0{,}5) \qquad (3)$$

Where, $\boldsymbol{r}$ is the bifurcation parameter. The chaotic behavior of the logistic map is visible when the bifurcation parameter $\boldsymbol{r}$ varies in the interval [3.57, 4]. Hence, using the abovementioned configuration, each period of carrier T_i is not a fixed value, it varies chaotically around $f_r = 20$kHz as a reference frequency. A detailed block diagram of the C-USPWM technique is depicted in Fig. 3. Chaotic triangular carrier signal generated by the simulated chaotic carrier schemes for a oH5 inverter and the waveform of chaotic period T_i are displayed.

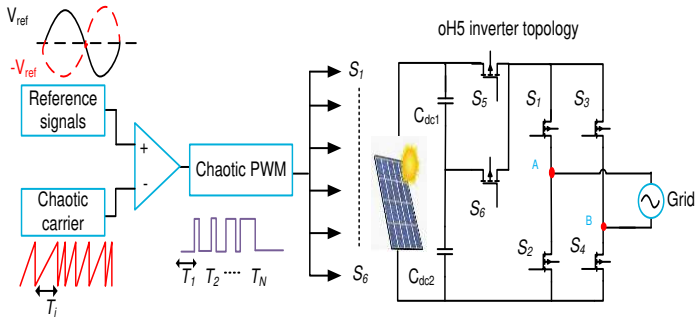

Fig. 3 Block diagram of chaotic USPWM technique for oH5 inverter.

3.1 *Different carrier waveforms*

A. *Low frequency study*

In this section, three different chaotic modulation technique has been implemented and investigated using different chaotic carrier waveforms: sawtooth carrier (Left-aligned), triangular carrier (Center-aligned), inverse sawtooth carrier (Right-aligned). As shown in Fig.4., the three signals are obtained with the same parameters of simulated schemes: β=0.3, T_r = 50 µs, $r = 4$ and $\gamma_0 = 0.3$.

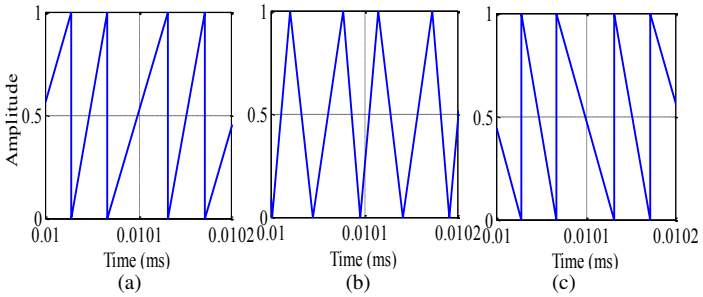

Fig. 4. Carrier waveforms: (a) chaotic sawtooth carrier (Left-aligned), (b) chaotic triangular carrier (Center-aligned) (c) inverse chaotic sawtooth carrier (Right-aligned).

The simulation results of output signal v_{AB} of each chaotic modulation signals, are shown in Fig.5. This validates the efficiency of the implementation of chaotic control. Compared to a conventional modulation, it is observed that there is a considerable reduction in the magnitude of harmonics. From the frequency spectrum in Fig. 2, note that harmonic peaks are concentrated at multiples of the switching frequency (around 20 kHz, 40 kHz, 60 kHz, etc.), but using different carrier waveforms, the CUPWM harmonics around the aforementioned frequencies have been distributed all over the frequency band. Obtained THD values for the studied control strategies are presented Fig.5. Regarding the frequency spectrum of the output voltage, there is a significant decrease in THD values with the different carrier forms. Using a sawtooth carrier and inverse sawtooth carrier, a decrease in THD by 22,2% and 23,7% respectively has been obtained. However using a triangular carrier, there is a very promising reduction in THD of about 40.6%. In this case, obtained results from the chaotic triangular carrier control is more coherent and robust. Consequently, it is recommended to implement a chaotic

USPWM using triangular carrier as a control technique in particular for oH5 PV inverter.

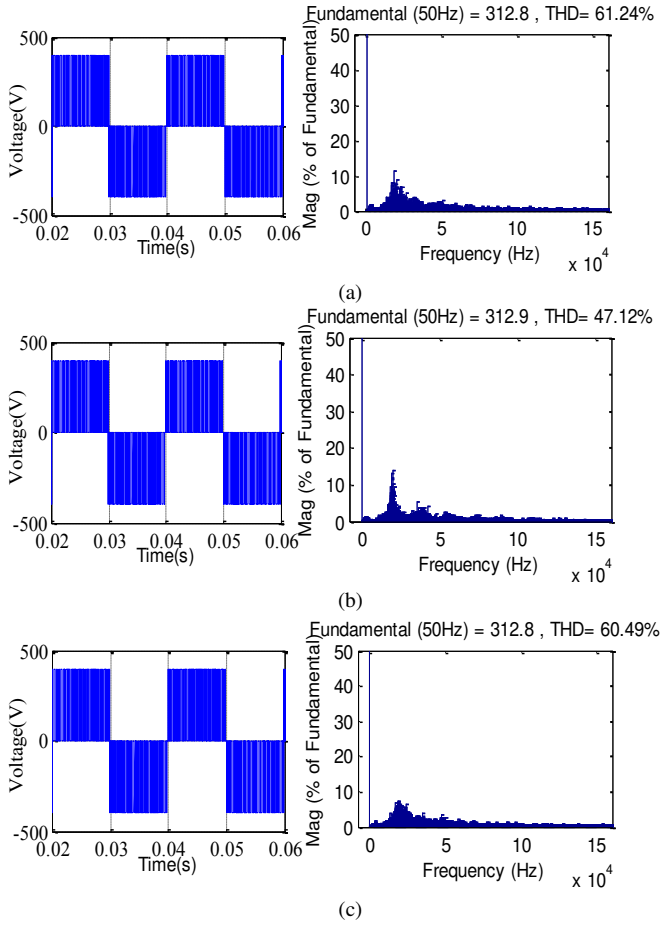

Fig. 5. Output results under C-USPWM control using (a) sawtooth carrier, (b) triangular carrier, (c) inverse sawtooth carrier

B. High frequency investigation

In order to study the effect of different USPWM control strategies on conducted disturbances over a wide frequency band, a high frequency (HF) model of the studied oH5 transformerless PV inverter has been carried out [21] [22]. This can be achieved through considering all parasitic inductances and stray capacitances to ground of the system. In particular, the layout of the printed circuit board (PCB) of the studied structure is required to identify the stray elements of the PCB tracks. In addition to parasitic capacitances between transistors and the grounded heatsink, the parasitic inductances of the drain and the source of the six MOSFET model have to be taken into account. The value of these stray elements can be easily obtained from datasheets. Furthermore, in order to measure CM voltage, a line impedance stabilized network (LISN) is inserted between the AC terminals of the studied oH5 and the grid.

Numerical HF model of the oH5 inverter when connected to the grid through a LISN filter has been implemented using a circuit-type software running with a 10 ns simulation time step. Thereafter, the generation of control signals of the transistor gates based on the different aforementioned unipolar SPWM techniques has been performed using the Simulink environment. Hence, a co-simulation of circuit-type based software and Matlab/simulink has been achieved coupling options of an electromagnetic field solver, providing a precise physics-based modeling environment, and the ease of control algorithms implementation. The proposed co-simulation interface combining the two software environments perfectly serves the needs for the present EMI study with offering powerful tools of time and frequency domains analysis for power electronics systems. Data exchange is achieved through dialog boxes implemented in both environments. In the circuit software interface, a "Simulink Component" block has been created for communication and signals exchange.

Based on the proposed co-simulation, the complete studied structure under the control of the three aforementioned carrier waveforms has been simulated and the CMV has been obtained at the terminals of the LISN. Fig. 6 shows a comparison between the three chaotic carrier waveforms. These results show that the three strategies give practically the same performances in terms of conducted EMI. Compared to conventional USPWM in Fig.7, the chaotic triangular carrier control that ensure the minimum THD provides an important reduction of the peak's amplitude of the CM emissions by approximately 10 dBμV at the switching frequency and its multiples.

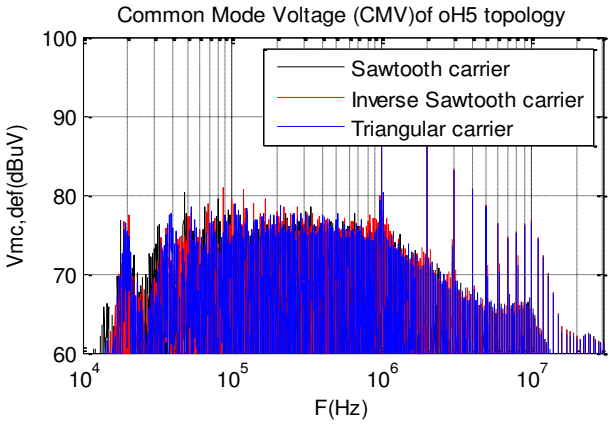

Fig. 6. Frequency spectra of conducted EMI obtained with numerical simulation and provided by different carrier waveforms

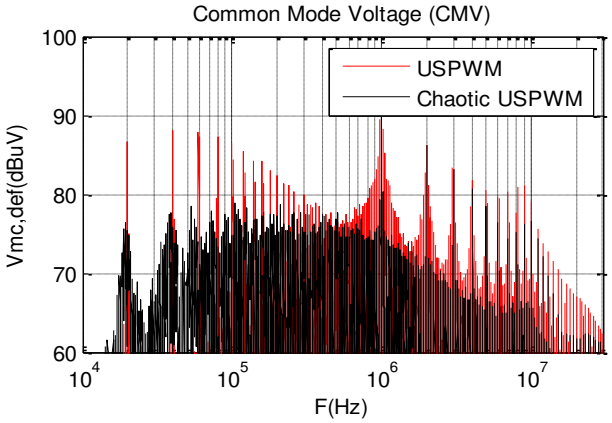

Fig. 7. Frequency spectra of the CM voltage in oH5 inverter obtained with numerical simulation

3.2 Parameter selection

C-USPWM introduces the Chaos concept into traditional modulation technique. In this modulation technique, the chaotic triangular carrier plays a key role, since the distribution of voltage harmonics is affected by parameters of the chaotic scheme. Hence, the β parameter identifies the varying width of the PWM technique. The methodology to select the β parameter of the triangular carrier is to make a sequence of simulation tests with different values of β. We can note if β=0, we are in the case of conventional USPWM with constant switching frequency. In order to estimate the most appropriate β parameter, a series of simulation tests are carried out to determine the THD of the output voltage corresponding to each β parameter value as shown by Fig.8. For β = 0.05, the triangular signal begins to vary chaotically. As well, we notice that the harmonic peak begins to attenuate compared with those obtained by conventional USPWM. It is clear that the C-USPWM with β=0.3 provides a significant reduction in the THD value by 66.5%, without neglecting the considerable reduction of the harmonic peak amplitude at the switching frequency and its multiples by spreading the energy spectrum over a wide frequency band. However, we notice from Fig.8 (c) that the THD starts to increase again for β = 0.4. Comparing to constant switching technique (USPWM), the proposed triangular chaotic control with parameter β=0.3 can easily reduce the EMI at low frequencies and decrease significantly the THD of the modulated output voltage.

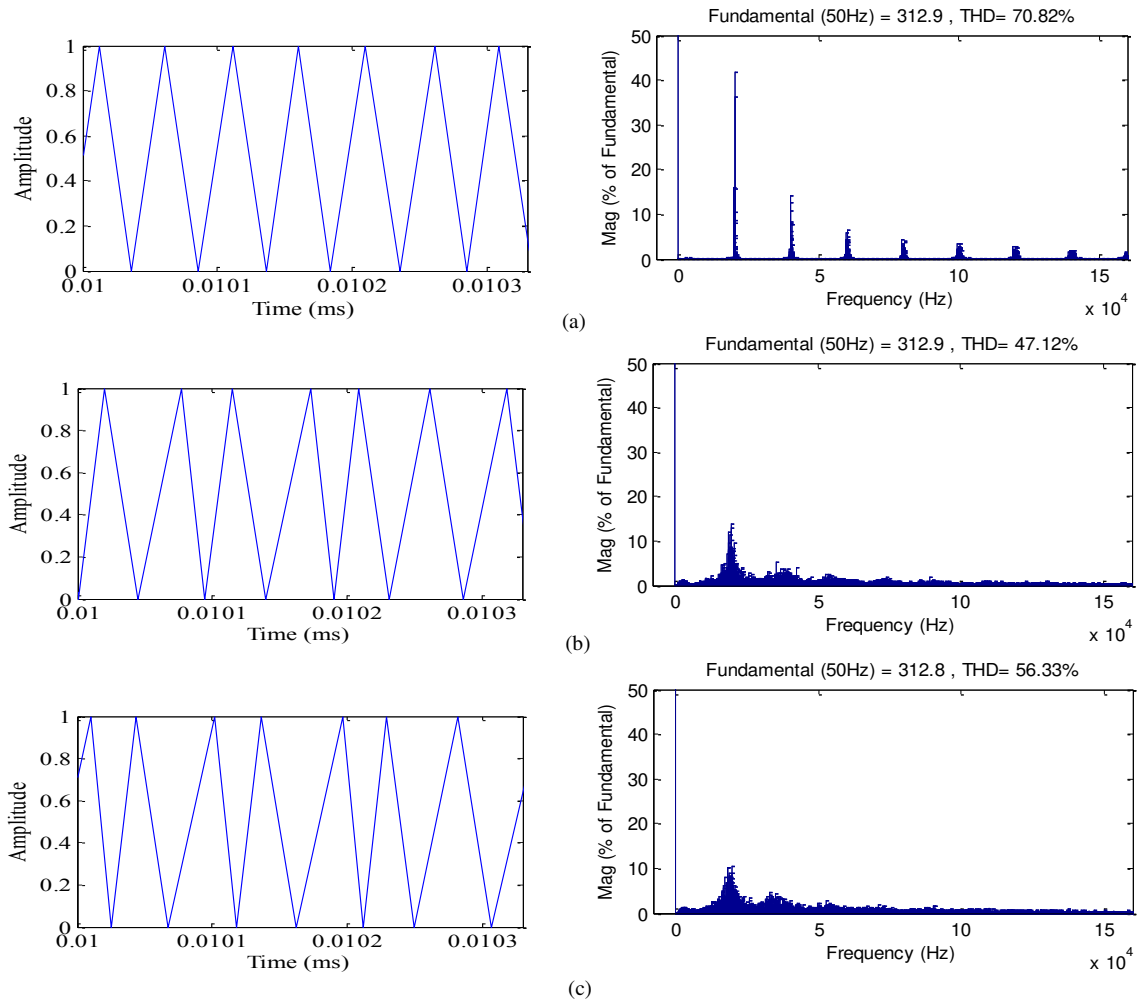

Fig. 8. Numerical simulation results of chaotic carrier waveforms and the FFT analysis for output voltage (v_{AB}) with (a) β = 0.05, (b) β = 0.3, (c) β = 0.4

4. Real time implementation of the chaotic USPWM

In this work, an original C-USPWM implementation method is proposed using a DSP TMS 320F28335 of Texas Instruments for real time processing. In fact, the chaos signal generation is performed using a co-simulation interface of Code composer studio software and Matlab/Simulink environment without changing any configuration parameters of the control board. Fig. 9 sketches the main steps to construct control signals for C-USPWM. First, the chaotic scheme is implemented using Simulink to generate a non-constant carrier period T_c that is changing chaotically. To generate a chaotic carrier, we designed the counters of the epwm modules to work with a variable period. The latter can simply be achieved through the appropriate configuration of the TMPRD register. Moreover, to provide a triangular carrier, the counters in each epwm module

are operating in a continuous up-down mode. Finally, the gates pulses are generated by comparing the instantaneous values of the counter registers to the instaneous amplitude of the modulation signal. For instance, at each rising edge, the output signal of the counter is compared to the reference signal associated to S1. Then, the result of this comparison is routed to the gate of S1 through a dedicated turn-on delay block to determine the appropriate dead-time. The gating pulse of S2 is obtained by applying a turn-off delay and a logical inversion to the first output signal of the comparison register. Similar approach is implemented for the rest of switches. Finally, a real-time workshop of Simulink generates the executable code and downloads it in the memory of the DSP in order to control the oH5 power circuit.

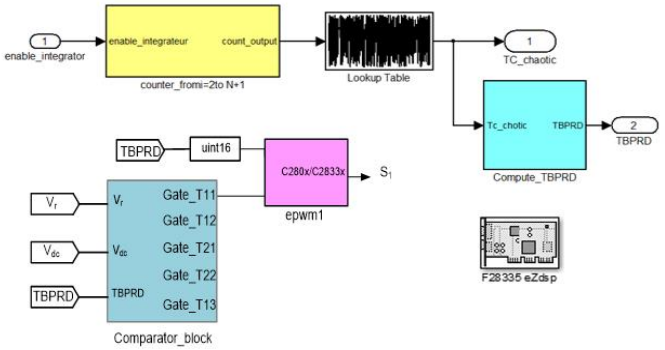

Fig. 9. Implementation of C-USPWM scheme using co-simulation.

4.1 *Obtained experimental results*

With the aim to validate previous simulation results, the conventional and the chaotic unipolar SPWM techniques with different parameter value of β are performed and investigated using the laboratory prototype of a transformerless oH5 grid-connected PV inverter based on a DSP real time implementation. The test prototype is illustrated in Fig.10.
Fig. 11 displays measured grid currents (i_g) and emission voltages v_{R1} and v_{R2} across the LISN and under the control of conventional USPWM, then C-USPWM. Conducted emissions (v_{R1}, v_{R2}) are measured in time domain using a high precision oscilloscope to determine CM voltage. Thus, the frequency domains results can be obtained by simply applying a fast Fourier transform (FFT) to time-domain conducted EMI. Frequency-domain results are distributed in the band 150 kHz to 30 MHz. as depicted in Fig. 12. Moreover, Figs. 13 show THD values of the output voltage v_{AB} under the conventional USWPM and C-USPWM. For C-USPWM, we present two tests with different β values.

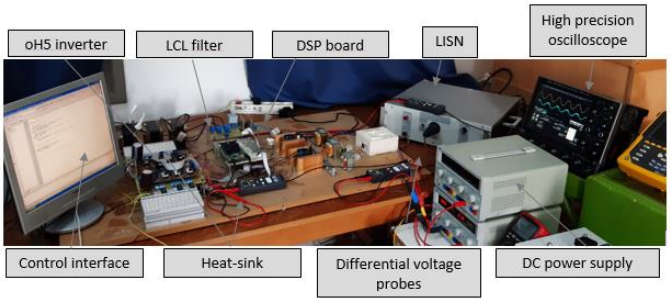

Fig. 10. In-lab conducted emission test stand of single-phase transformerless grid-connected PV inverter.

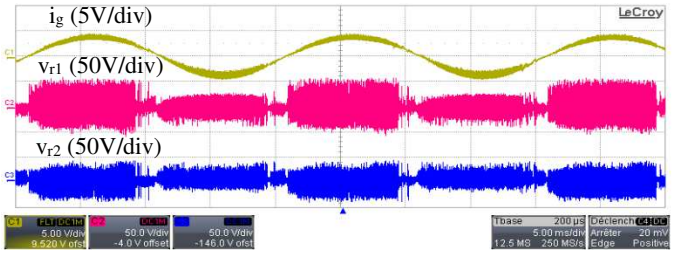

(a)

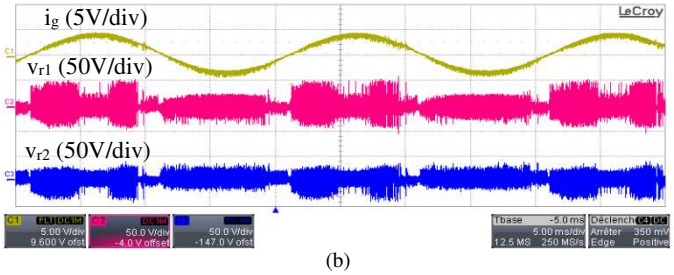

(b)

Fig. 11. Obtained experimental results: (a) under USPWM control (b) under C-USPWM control.

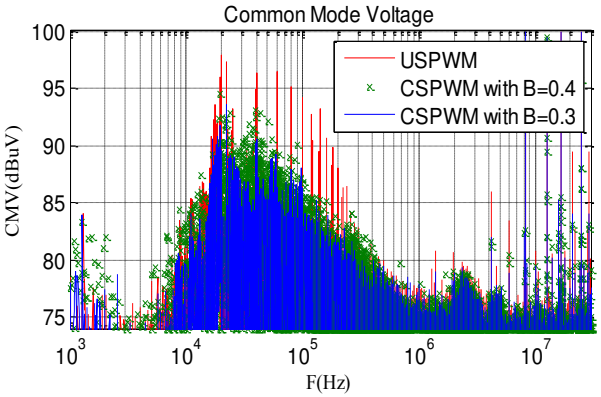

Fig.12. Experimental frequency spectrum of conducted emission provided by oH5 inverter under USPWM (red) and C-USPWM (green and blue).

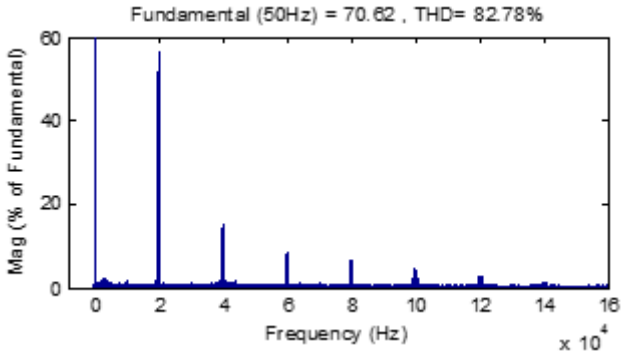

(a)

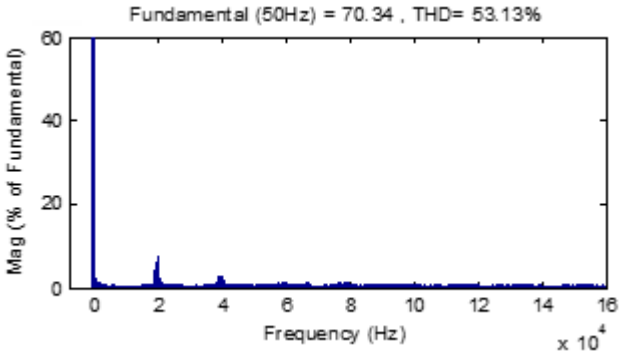

(b)

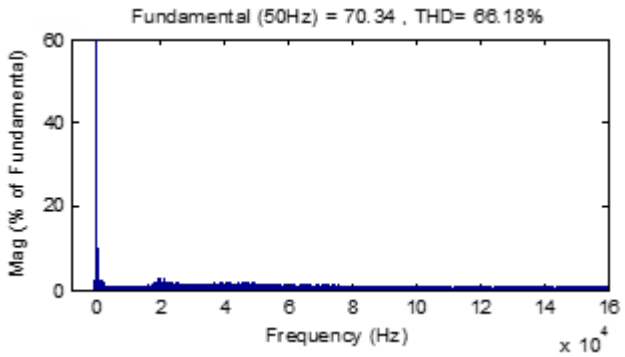

(c)

Fig.13. Measured harmonic spectrum of Output voltage v_{AB} (a) under USPWM control (b) under C-USPWM control with β = 0.3, (c) under C-USPWM control with β = 0.4

4.1 Discussion

The constant carrier frequency of conventional USPWM causes high harmonic peaks in the switching frequency and its multiples. These harmonics are dangerous and can result in serious conducted EMI. Therefore, the use of variable carrier frequency is highly recommended. It can be concluded from the above experimental results (Fig.11) that chaotic USPWM-based strategies have no concerns with the performance of transformerless single-phase grid-connected PV inverters.

However, comparing with conventional USPWM, C-USPWM provide a significant reduction in the amplitude of harmonic peaks at the carrier frequency and its multiples by distributing the energy spectrum.

Fig. 12 shows the spectrum of the output CM voltage that has been obtained at the terminals of the LISN under conventional USPWM and CUSWM. As it can be noticed when comparing to standard USPWM technique, C-USPWM with the two different values of β ensure a significant reduction in the amplitude of the harmonic peaks at the carrier frequency (20KHz) and its multiples. Therefore, for grid-connected PV inverters, this modulation technique can be good alternatives to reduce EMI without adding any additional bulky and heavy devices or components especially in low frequencies.

Obtained THD results of the output voltage v_{AB} for the studied control strategies are shown in Fig.13. Compared to traditional reference strategy (Fig.13 (a)) there is a significant decrease in THD values by 35.8% under chaotic strategies when β value is equal to 0.3. Fig.13 (c) shows that the THD value starts to increase under the C-USPWM with β = 0.4. Despite in this case, the harmonic peaks are spread over the frequency range and the harmonic magnitude is significantly reduced. Therefore, a higher value of β contributes to increase THD value and worsening the power quality. Hence, this parameter should be carefully chosen to make a compromise between performance in terms of THD and conducted EMI provided by transformerless PV inverters. It is clear that simulation and experimental results have the same tendency despite the little difference due to several causes such as the accuracy of estimated HF modelling. Obtained results validate the efficiency of the real-time implementation and highlights the pertinence of the parameter selection in the chaotic modulation control.

5. Conclusion

This paper proposed and implemented a C-USPWM algorithm for a transformerless single-phase grid-connected PV inverter. The main benefit of this proposed technique as compared to the conventional USPWM method is the reduction of the conducted EMI level. This benefit was achieved with a THD improvement if the appropriate parameters are selected. The principle of implementing the proposed techniques is introduced and verified through simulation and experiment. Experimental real-time implementation results have been obtained using a lab prototype of a oH5 inverter. It has been proven that at low frequencies, the C-USPWM method has considerably mitigated the conducted emissions and provided a good performance in terms of injected grid current quality (THD) with no extra EMI filtering components added for transformerless single-phase grid-connected PV inverter.

REFERENCES

[1] Kirthiga S, Jothi Swaroopan N.M. Highly reliable inverter topology with a novel soft computing technique to eliminate leakage current in grid-connected transformerless photovoltaic systems. *Comput. Electr. Eng* 2018; *68*: 192–203.

[2] Khan MNH, Forouzesh M, Siwakoti YP, Li L, Kerekes T and Blaabjerg F. Transformerless Inverter Topologies for Single-Phase Photovoltaic Systems: A Comparative Review. *IEEE J. Emerg. Sel. Topics Power Electron 2020; 8: 80*5-835.

[3] Victor M, et al. Method of converting a direct current voltage from a source of direct current voltage, more specifically from a photovoltaic source of direct current voltage, into an alternating current voltage. *US Patent*7411802 2008.

[4] Islam M, Mekhilef S. H6-type transformerless single-phase inverter for grid-tied photovoltaic system. *IET Power. Electron* 2015; 8(4): 636–644.

[5] Zhang L, Sun K, Feng L, Wu H and Xing Y. A Family of Neutral Point Clamped Full-Bridge Topologies for Transformerless Photovoltaic Grid-Tied Inverters. *IEEE Trans on Power Electron 2013;* 28(2): 730-739.

[6] Xiao *H, Xie S, Chen Y and Huang R.* An Optimized Transformerless Photovoltaic Grid-Connected Inverter. *IEEE Trans on Industrial Electron 2011; 58(5):1887-1895.*

[7] Pellitteri F, *et al*. A prototypal PCB board for the EMI characterization of SiC-based innovative switching devices. In: *20th Mediterranean Electrotechnical Conference (MELECON)*; 2020, p. 52-56. June 16-18.

[8] Zhang Z, Hu Y, Chen X, Jewell GW, Li H. A Review on Conductive Common-Mode EMI Suppression Methods in Inverter Fed Motor Drives. *IEEE Access* 2021; 9: 18345-18360.

[9] Belloumi W, Bréard A, Ben Hadj Slama J and Vollaire C. Impact of Layout on the Conducted Emissions of a DC-DC Converter Using Numerical Approach. In: *15th International Multi-Conference on Systems, Signals & Devices (SSD) 2018,* p. 287-291. March 19-22.

[10] Salem M, Hamouda M, Ben Hadj Slama J. Comparative study of conventional modulation schemes in terms of conducted and radiated emi generated by three-phase inverters. *Turk .J. Electr Eng 2017;* 25,(3):1599-1611.

[11] Satish Kumar M, Jhansi Rani A. Reduction of conducted electromagnetic interference by using filters. *Comput. Electr. Eng 2018; 72:* 169–178.

[12] Bhargava A, Pommerenke D, Kam KW, Centola F, Lam CW. DC-DC buck converter EMI reduction using PCB layout modification. IEEE Trans on Electromagnetic Compatibility 2011; 53(3): 806-813.

[13] Li W, Gu Y, Luo H, Cui W, He X, and Xia C. Topology Review and Derivation Methodology of Single-Phase Transformerless Photovoltaic Inverters for Leakage Current Suppression. IEEE Trans on Industrial Electron 2015; 62(7): 4537-4551.

[14] Jiang D, Chen J, Shen Z. Common mode EMI reduction through PWM methods for three-phase motor controller. CES Transactions on Electrical Machines and Systems 2019; 3(2): 133-142.

[15] Chen J, Jiang D, Shen Z, Sun W and Fang Z. Uniform Distribution Pulse width Modulation Strategy for Three-Phase Converters to Reduce Conducted EMI and Switching Loss. *IEEE Trans on Industrial Electron 2020*; 67(8): 6215-6226.

[16] Zhang Z, Wei L, Yi P, Cui Y, Murthy PS, Bazzi AM. Conducted Emissions Suppression of Active Front End (AFE) Drive Based on Random Switching Frequency PWM. IEEE Trans on Industry Applications 2020; 56(6): 6598-6607.

[17] Kraiem S, Hamouda M and Ben Hadj Slama J. EMI Reduction in Transformerless Photovoltaic Grid-Connected Inverter via Chaotic SPWM Control. In*: 6th IEEE International Energy Conference (ENERGYCon)*; 2020, p. 210-215. 28 Sept.-1 Oct

[18] Zhang B, and Wang X. Chaos analysis and chaotic EMI suppression of DC-DC converters. John Wiley & Sons 2014.

[19] Li H, Liu Y, Lü J, Zheng T and Yu X. Suppressing EMI in Power Converters via Chaotic SPWM Control Based on Spectrum Analysis Approach. *IEEE Trans on Industrial Electron 2014;* 61(11): 6128-6137.

[20] Lamb J, Mirafzal B. An adaptive SPWM technique for cascaded multilevel converters with time-variant DC sources. IEEE Trans on Industry Applications 2016; 52(5): 4146-4155.

[21] Kraiem S, Hamouda M, Ben Hadj Slama J. Conducted EMI mitigation in transformerless PV inverters based on intrinsic MOSFET parameters. *Microelectronics Reliability 2020;*114.

[22] Kraiem S, Hamouda M, Ben Hadj Slama J. Electromagnetic interference-based comparative study between transformerless H5 and optimised H5 grid-connected photovoltaic inverters. *in IET Sci Meas Technol 2021;*15(4): 343– 351.